Electronic supplementary information (ESI) for

Field-induced slow magnetic relaxation of octahedrally coordinated mononuclear Fe(III)-, Co(II)-, and Mn(III)-containing polyoxometalates

Rinta Sato, Kosuke Suzuki,* Takuo Minato, Masahiro Shinoe, Kazuya Yamaguchi and Noritaka Mizuno*
Department of Applied Chemistry, School of Engineering, The University of Tokyo, 7-3-1 Hongo, Bunkyo-ku, Tokyo 113-8656 (Japan)

General: IR spectra were measured on JASCO FT/IR-4100 using KBr disks. Cold-spray ionization (CSI) mass spectra were recorded on JEOL JMS-T100CS. Thermogravimetric and differential thermal analyses (TG-DTA) were performed on Rigaku Thermo plus TG 8120. ICP-AES analyses were performed with Shimadzu ICPS-8100. Elemental analyses for C, H, N were performed on a Yanaco MT-6 at the Elemental Analysis Center of School of Science (the University of Tokyo). UV-Vis spectra were measured on JASCO V-570 using 1 cm quartz cell. $TBA_4H_6[A\text{-}\alpha\text{-}SiW_9O_{34}]\cdot 2H_2O$ was synthesized according to the reported procedure.[S1] $Fe(acac)_3$ and $Mn(acac)_3$ were obtained from TCI. $Co(acac)_2\cdot 2H_2O$ was obtained from Kanto Chemical. Solvents were obtained from Wako Pure Chemical Industries and Kanto Chemical and used as received.

X-ray crystallography: Diffraction measurements were made on a Rigaku MicroMax-007 Saturn 724 CCD detector with graphite monochromated Mo Kα radiation (λ = 0.71069 Å) at 123 K. The data were collected and processed using CrystalClear[S2] and HKL2000.[S3] Neutral scattering factors were obtained from the standard source. In the reduction of data, Lorentz and polarization corrections were made. The structural analyses were performed using CrystalStructure,[S4] WinGX,[S5] and Yadokari-XG.[S6] All structures were solved by SHELXS and refined by full-matrix least-squares methods using SHELXL-97.[S7] The metal atoms (Si, W, Fe, Co, Mn) and oxygen atoms in the POM frameworks were refined anisotropically. CCDC-1035329 ($\mathbf{I_{Fe}}$), CCDC-1035330 ($\mathbf{I_{Co}}$), and CCDC-1035331 ($\mathbf{I_{Mn}}$) contain the supplementary crystallographic data for this paper. The data can be obtained free of charge via www.ccdc.cam.ac.uk/conts/retrieving.html (or from the Cambridge Crystallographic Data Centre, 12, Union Road, Cambridge CB2 1EZ, UK; Fax: (+44) 1223-336-033; or deposit@ccdc.cam.ac.uk).

Bond valence sum (BVS) calculations: The BVS values were calculated by the expression for the variation of the length r_{ij} of a bond between two atoms i and j in observed crystal with valence V_i:

$$V_i = \sum_j \exp\left(\frac{r_0' - r_{ij}}{B}\right)$$

where B is constant equal to 0.37 Å, r'_0 is bond valence parameter for a given atom pair.[S8]

Magnetic Measurements: Magnetic susceptibility data of the polycrystalline samples were measured on Quantum Design MPMS-XL7. Dc magnetic susceptibility measurements were carried out under the applied field of 0.1 T in the temperature range of 1.9–300 K. Variable-field (1–7 T) magnetization measurements were carried out in the temperature range of 1.9–10 K. Ac magnetic susceptibility measurements were carried out under the 3.96 Oe ac oscillating field. Diamagnetic corrections were applied by using Pascal constants and diamagnetisms of the sample holder and $TBA_4H_6[A\text{-}\alpha\text{-}SiW_9O_{34}]\cdot 2H_2O$.

Electron Spin Resonance (ESR) Spectrum: ESR spectrum as recorded on JEOL JES-X320 equipped with a liquid helium variable temperature controller (ES-CT470) at 4.2 K (9.07 GHz). Spectrum was simulated using Hyperfine 2.52 program[S9] with the following effective spin Hamiltonian:

$$H' = \mu_B \left(g'_x H_x S'_x + g'_y H_y S'_y + g'_z H_z S'_z \right) + A'_x I_x S'_x + A'_y I_y S'_y + A'_z I_z S'_z$$

where the first term accounts for the Zeeman interaction and the last three account for the hyperfine interaction with ^{59}Co (I = 7/2). The pattern in Fig. S5 was simulated using the following values: g'_x = 3.31, g'_y = 6.76, g'_z = 1.83 and $A'_x = 68\times10^4$ cm^{-1}, $A'_y = 240\times10^4$ cm^{-1}, $A'_z = 76\times10^4$ cm^{-1}.

Synthesis of $\mathbf{I_{Fe}}$: To a mixed solvent of acetone and water (5.76/0.24 mL) of $Fe(acac)_3$ (10.9 mg, 30.9 μmol), $TBA_4H_6[A\text{-}\alpha\text{-}SiW_9O_{34}]\cdot 2H_2O$ (200 mg, 61.8 μmol, 2.0 equiv. with respect to $Fe(acac)_3$) was added, and the resulting solution was stirred for 5 h at room temperature (ca. 20°C). Then, diethyl ether (20 mL) was added. Pale yellow precipitates formed were filtered off (172 mg), followed by recrystallization from mixed solvent of 1,2-dichloroethane and diethyl ether. The pale yellow crystals of $\mathbf{I_{Fe}}$ suitable for X-ray crystallographic analysis were obtained (79.2 mg, 40% yield based on $TBA_4H_6[A\text{-}\alpha\text{-}SiW_9O_{34}]\cdot 2H_2O$). Elemental analysis, calcd (%) for $C_{114}H_{270}Cl_2FeN_7O_{70}Si_2W_{18}$ ($TBA_7H_{10}[Fe(SiW_9O_{34})_2]\cdot 2H_2O\cdot C_2H_4Cl_2$): C, 21.56; H, 4.28; N, 1.54; Si, 0.88; Fe, 0.88; W, 52.10. Found: C, 21.50; H, 4.33; N, 1.47; Si, 0.88; Fe, 0.87; W, 52.36. Positive-ion MS (CSI, 1,2-dichloroethane): *m/z* 3333 (calcd. 3333) $[TBA_9H_6Fe(SiW_9O_{33})_2]^{2+}$, *m/z* 3453 (calcd. 3453) $[TBA_{10}H_5Fe(SiW_9O_{33})_2]^{2+}$, 6423 (calcd. 6423) $[TBA_8H_6Fe(SiW_9O_{33})_2]^{+}$. UV-Vis (acetonitrile): ε (λ) 29.1 M^{-1} cm^{-1} (400 nm). IR (KBr pellet): 1635, 1381, 1152, 1107, 1060, 1014, 992, 955, 889, 814, 772, 737, 683, 561, 524, 360, 338, 322, 302 cm^{-1}.

Synthesis of $\mathbf{I_{Co}}$: $\mathbf{I_{Co}}$ was synthesized via the same procedure as that for $\mathbf{I_{Fe}}$ except that $Co(acac)_2\cdot 2H_2O$ was used (orange crystals, 71% yield based on $TBA_4H_6[A\text{-}\alpha\text{-}SiW_9O_{34}]\cdot 2H_2O$). Elemental analysis, calcd (%) for $C_{114}H_{271}Cl_2CoN_7O_{70}Si_2W_{18}$ ($TBA_7H_{11}[Co(SiW_9O_{34})_2]\cdot 2H_2O\cdot C_2H_4Cl_2$): C, 21.54; H, 4.30;

N, 1.54; Si, 0.88; Co, 0.93; W, 52.07. Found: C, 21.28; H, 4.25; N, 1.53; Si, 0.89; Co, 0.94; W, 52.39. Positive-ion MS (CSI, 1,2-dichloroethane): *m/z* 3307 (calcd. 3307) $[TBA_9HCo(SiW_9O_{31})(SiW_9O_{32})]^{2+}$, *m/z* 3429 (calcd. 3429) $[TBA_{10}Co(SiW_9O_{31})(SiW_9O_{32})]^{2+}$, 6427 (calcd. 6427) $[TBA_8H_7Co(SiW_9O_{33})_2]^{+}$. UV-Vis (acetonitrile): ε (λ) 15.7 M^{-1} cm^{-1} (554 nm), 135 (400 nm). IR (KBr pellet): 1635, 1485, 1382, 1153, 1105, 1061, 995, 954, 898, 795, 765, 736, 624, 559, 522, 457, 374, 337 cm^{-1}.

Synthesis of $\mathbf{I_{Mn}}$ ($\mathbf{TBA_7H_{10}[Mn(SiW_9O_{34})_2]}$): To an acetone solution (4 mL) of $Mn(acac)_3$ (10.9 mg, 30.9 μmol), $TBA_4H_6[A\text{-}\alpha\text{-}SiW_9O_{34}]\cdot 2H_2O$ (200 mg, 61.8 μmol, 2.0 equiv. with respect to $Mn(acac)_3$) was added, and the resulting solution was stirred for 15 min at room temperature (ca. 20°C). Then, diethyl ether (1.4 mL) was added, and the resulting solution was kept at 30°C for 1 day. The yellow-green crystals of $\mathbf{I_{Mn}}$ were obtained (98.7 mg, 51% yield based on $TBA_4H_6[A\text{-}\alpha\text{-}SiW_9O_{34}]\cdot 2H_2O$). Elemental analysis, calcd (%) for $C_{112}H_{268}MnN_7O_{71}Si_2W_{18}$ ($TBA_7H_{10}[Mn(SiW_9O_{34})_2]\cdot 3H_2O$): C, 21.46; H, 4.31; N, 1.56; Si, 0.90; Mn, 0.88; W, 52.78. Found: C, 21.30; H, 4.25; N, 1.40; Si, 0.88; Mn, 1.00; W, 52.00. Positive-ion MS (CSI, acetone): *m/z* 3332 $[TBA_9H_6Mn(SiW_9O_{33})_2]^{2+}$ (*m/z* 3332), *m/z* 3453 $[TBA_{10}H_5Mn(SiW_9O_{33})_2]^{2+}$ (*m/z* 3453), *m/z* 6422 $[TBA_8H_6Mn(SiW_9O_{33})_2]^{+}$ (*m/z* 6422). UV-Vis (acetonitrile): ε (λ) 61.9 M^{-1} cm^{-1} (729 nm), 230 $M^{-1}cm^{-1}$ (442 nm). IR (KBr pellet): 1630, 1484, 1380, 1152, 1006, 957, 919, 875, 789, 534, 429, 378, 361, 313, 301, 293, 287, 271, 263, 252 cm^{-1}.

Table S1. Crystallographic data for $\mathbf{I_{Fe}}$, $\mathbf{I_{Co}}$, and $\mathbf{I_{Mn}}$

Compound	$\mathbf{I_{Fe}}$	$\mathbf{I_{Co}}$	$\mathbf{I_{Mn}}$
formula	$C_{116}Cl_4FeN_7O_{72}Si_2W_{18}$	$C_{124}Cl_{12}CoN_7O_{70}Si_2W_{18}$	$C_{114}MnN_7O_{74}Si_2W_{18}$
Fw (g mol^{-1})	6206.36	6557.12	6071.63
crystal system	monoclinic	triclinic	monoclinic
space group	$C2/c$ (#15)	P-1 (#2)	$C2/c$ (#15)
a (Å)	35.5945(2)	14.66160(10)	35.6567(2)
b (Å)	14.48620(10)	18.7039(2)	14.45530(10)
c (Å)	38.2599(2)	19.0694(2)	38.3421(3)
α (deg)	90	106.8644(4)	90
β (deg)	113.9049(3)	92.5856(4)	113.8849(3)
γ (deg)	90	98.2456(4)	90
V (Å^3)	18035.63(19)	4931.95(8)	18070.1(2)
Z	4	1	4
temp (K)	123(2)	123(2)	123(2)
ρ_{calcd} (g cm^{-3})	2.286	2.208	2.232
GOF	1.115	1.081	1.116
R_1 [$I>2\sigma(I)$]	0.0424 (for 16341 data)	0.0616 (for 23030 data)	0.0469 (for 17846 data)
wR_2	0.0994 (for all 17087 data)	0.1526 (for all 24985 data)	0.1156 (for all 18464 data)

Table S2. Selected bond lengths and angles for $\mathbf{I_{Fe}}$, $\mathbf{I_{Co}}$, and $\mathbf{I_{Mn}}$

Bond lengths (Å)			
	$\mathbf{I_{Fe}}$	$\mathbf{I_{Co}}$	$\mathbf{I_{Mn}}$
M1–O1	2.003(6)	2.044(8)	1.928(5)
M1–O2	1.991(6)	2.065(7)	1.939(5)
M1–O19	2.098(6)	2.193(7)	2.223(5)
O1···O3*	2.668(6)	2.618(8)	2.753(6)
O2···O6*	2.687(8)	2.695(7)	2.736(7)
O5···O6	2.71(1)	2.75(2)	2.677(8)
O4···O35	2.72(1)	2.69(2)	2.723(9)
O5···O35	2.63(2)	2.72(1)	2.62(1)
Angles (deg)			
	$\mathbf{I_{Fe}}$	$\mathbf{I_{Co}}$	$\mathbf{I_{Mn}}$
O1–M1–O2	91.3(2)	87.0(3)	88.2(2)
O1–M1–O19	79.8(2)	76.9(3)	77.75(19)
O2–M1–O19	100.0(2)	101.4(3)	101.36(19)

Table S3. Selected BVS values for $\mathbf{I_{Fe}}$, $\mathbf{I_{Co}}$, and $\mathbf{I_{Mn}}$

	$\mathbf{I_{Fe}}$	$\mathbf{I_{Co}}$	$\mathbf{I_{Mn}}$		$\mathbf{I_{Fe}}$	$\mathbf{I_{Co}}$	$\mathbf{I_{Mn}}$
W1	6.13	6.20	6.09	M1	2.90	2.02	3.08
W2	6.17	6.13	6.09	Si1	3.97	3.99	3.94
W3	6.16	6.01	6.10	O1	1.71	1.48	1.76
W4	6.19	6.01	6.13	O2	1.78	1.34	1.78
W5	6.17	6.04	6.14	O3	0.53	0.85	0.50
W6	6.18	6.14	6.12	O4	1.50	0.83	1.52
W7	6.19	6.11	6.05	O5	0.52	0.85	0.50
W8	6.14	6.09	6.06	O6	0.90	0.70	0.88
W9	6.02	6.03	6.04	O19	1.94	1.89	1.94

Table S4. Relaxation times τ (s) and α values for $\mathbf{I_{Fe}}$ under the external dc field of 0.1 T

T / K	τ / s	α
1.90	0.002703	0.08
1.95	0.002273	0.07
2.00	0.002004	0.07
2.05	0.001724	0.06
2.10	0.001515	0.04
2.20	0.001282	0.05
2.30	0.001111	0.05
2.40	0.001000	0.03
2.50	0.000833	0.03

Table S5. Relaxation times τ (s) and α values for $\mathbf{I_{Co}}$ under the external dc field of 0.1 T

T / K	τ / s	α
2.00	0.031250	0.066
2.50	0.021739	0.07
3.00	0.012500	0.06
4.00	0.005464	0.06
5.00	0.002500	0.04
6.00	0.001250	0.05

Table S6. The angle distortion parameters of Co(II) in $\mathbf{I_{Co}}$ and the reported octahedrally coordinated mononuclear Co(II) SMMs

Compound [a]	Coordinating atoms	Angle distortion (A) [b]	D / cm^{-1}	E / cm^{-1}	ref
$\mathbf{I_{Co}}$	O6	10.19	95.2	7.18	this work
$Co(acac)_2(H_2O)_2$	O6	1.54	57	17.7	16e
1	N6	1.03	–	–	16a
2	N6	7.22	98	8.4	16b
3	N3O3	8.50	41.7	1.6	16c
4	N6	5.66	24.6	13.0	16d

[a] **1**, $[Co(SCN)_2 \cdot \{4\text{-}(\alpha\text{-diazobenzyl})pyridine\}_4]$; **2**, *cis*-$[Co(dmphen)_2(NCS)_2]\cdot 0.25EtOH$ (dmphen = 2,9-dimethyl-1,10-phenanthroline); **3**, $[Co(\mu\text{-L})(\mu\text{-OAc})Y(NO_3)_2]$; **4**, $[Co(abpt)_2(tcm)_2]$ (abpt = 4-amino-3,5-bis(2-pyridyl)-1,2,4-triazole; tcm = tricyanomethanide anion). [b] Angle distortion (A) was calculated by the following equation, where N, a_m, and a_i are the number of bonds, the mean angles, and the individual angles, respectively:

$$A = \frac{100}{N} \cdot \sum_{i=1}^{N} \frac{|a_i - a_m|}{a_m}$$

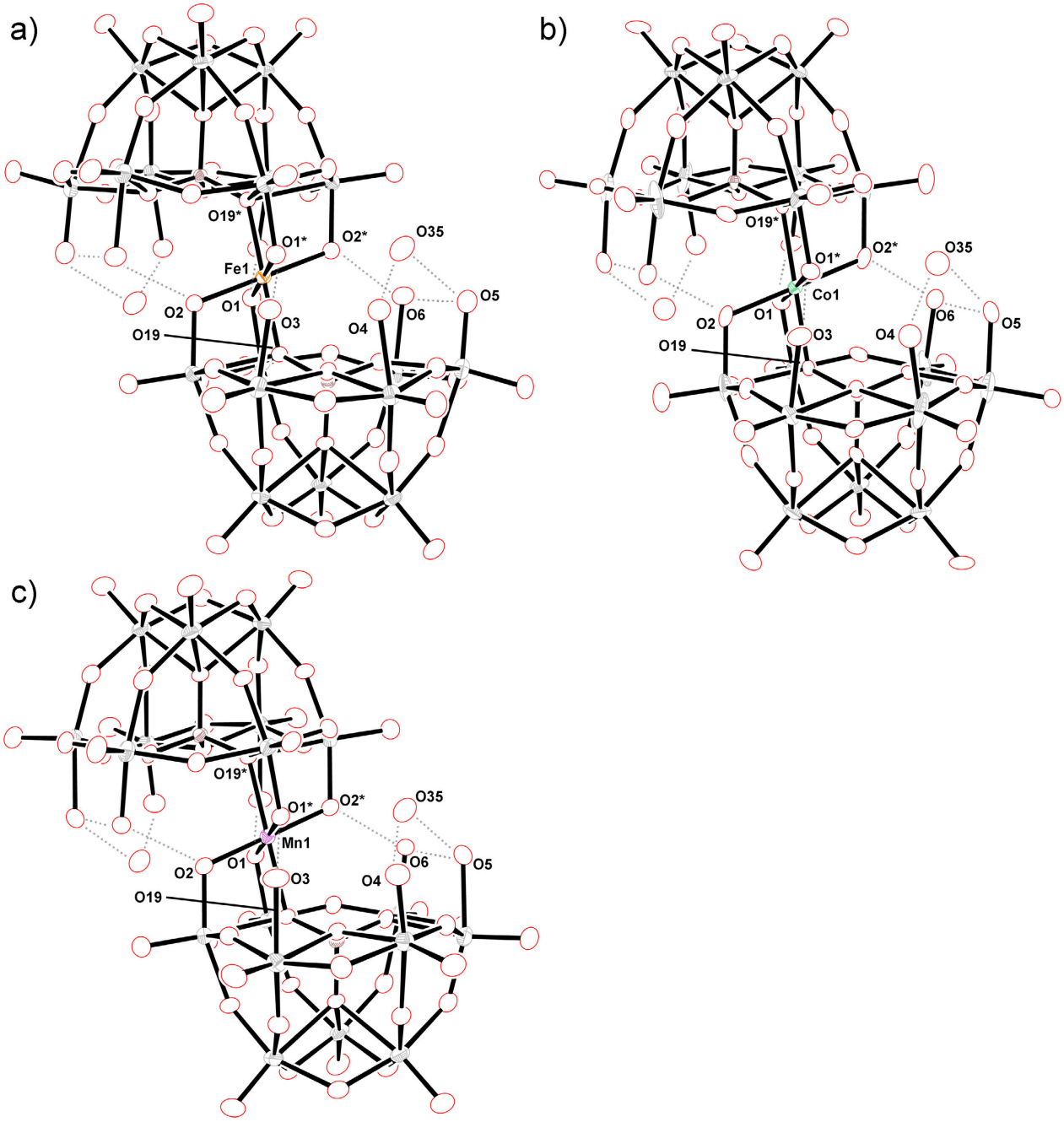

Fig. S1. ORTEP representations with thermal ellipsoids drawn at the 50% probably level of the anion parts of (a) $\mathbf{I_{Fe}}$, (b) $\mathbf{I_{Co}}$, and (c) $\mathbf{I_{Mn}}$. The dotted lines indicate the hydrogen bonding networks.

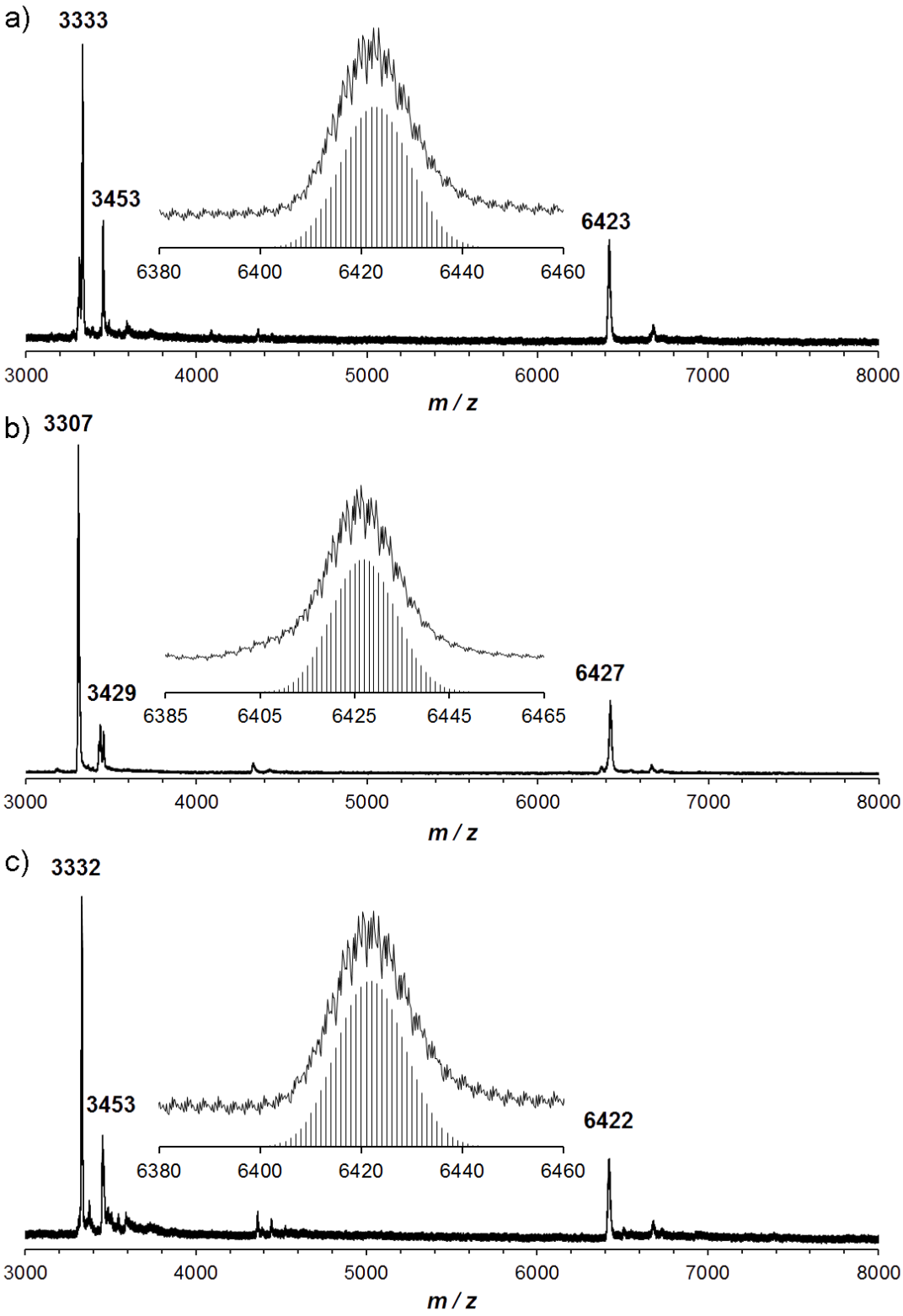

Fig. S2. Positive-ion CSI-mass spectra of (a) $\mathbf{I_{Fe}}$, (b) $\mathbf{I_{Co}}$, and (c) $\mathbf{I_{Mn}}$ in DCE. Inset: (a) spectrum in the range of *m/z* 6380–6460 and the simulated pattern for $[TBA_8H_6Fe(SiW_9O_{33})_2]^+$ (*m/z* 6423), (b) spectrum in the range of *m/z* 6385–6465 and the simulated pattern for $[TBA_8H_7Co(SiW_9O_{33})_2]^+$ (*m/z* 6427), and (c) spectrum in the range of *m/z* 6380–6460 and the simulated pattern for $[TBA_8H_6Mn(SiW_9O_{33})_2]^+$ (*m/z* 6422).

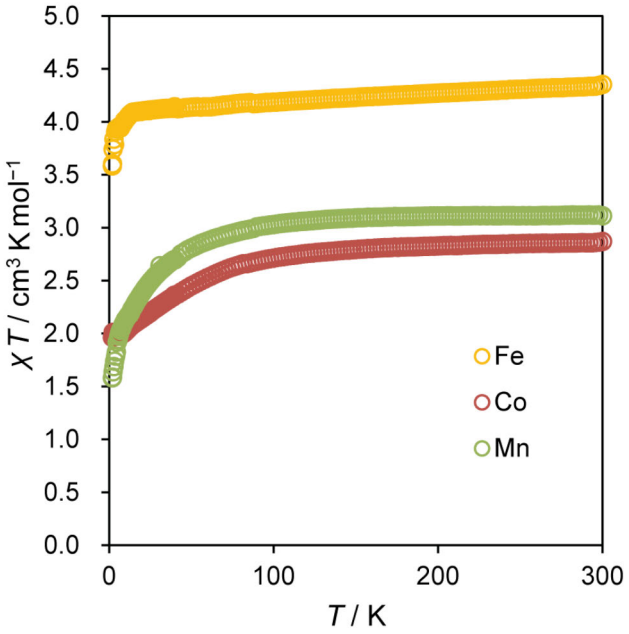

Fig. S3. Temperature dependence of χT for $\mathbf{I_{Fe}}$, $\mathbf{I_{Co}}$, and $\mathbf{I_{Mn}}$ under the applied field of 0.1 T.

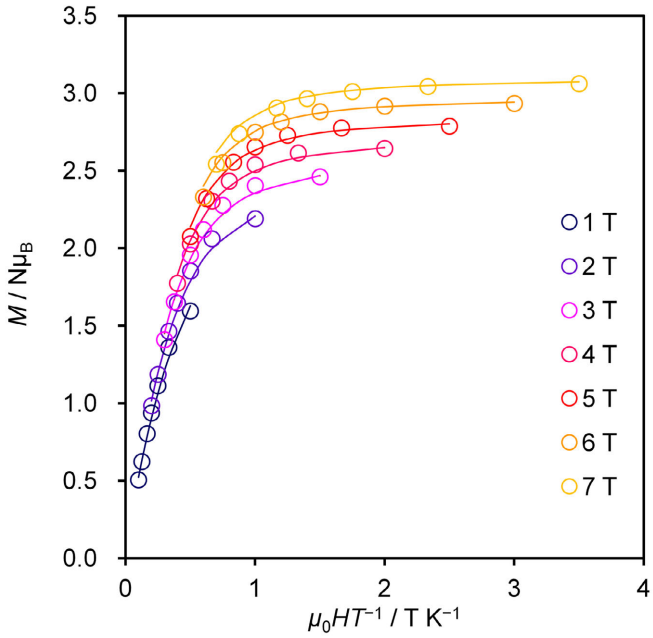

Figure S4. Low-temperature magnetization data for $\mathbf{I_{Mn}}$ collected in the temperature range of 1.9–10 K under the external dc field of 1–7 T. Solid lines represent the best fits obtained with PHI program.

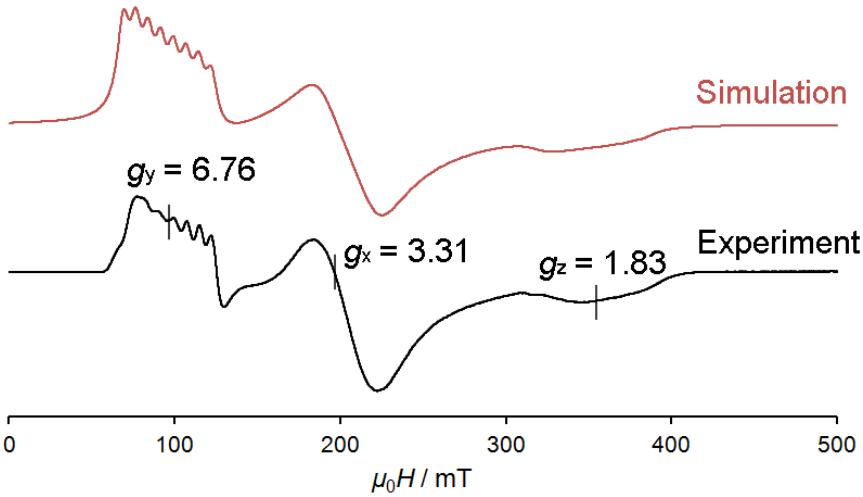

Fig. S5. X-band ESR spectrum of the polycrystalline sample of $\mathbf{I_{Co}}$ at 4.2 K and the simulation pattern.

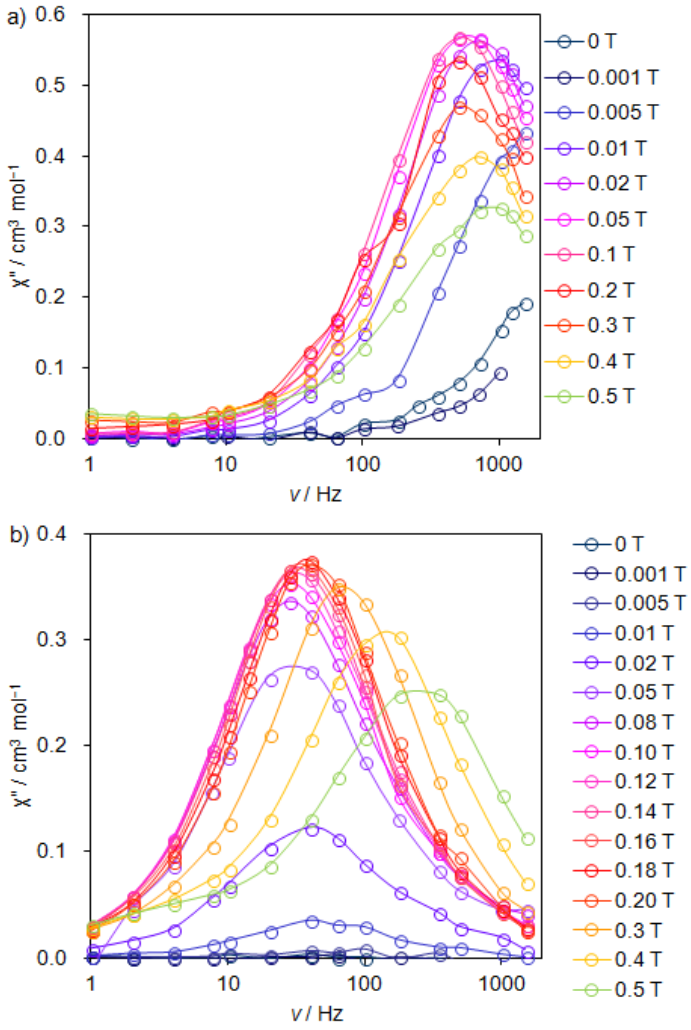

Fig. S6. Frequency dependence of χ'' for (a) $\mathbf{I_{Fe}}$ and (b) $\mathbf{I_{Co}}$ under the external dc field in the range of 0–0.5 T at 2 K.

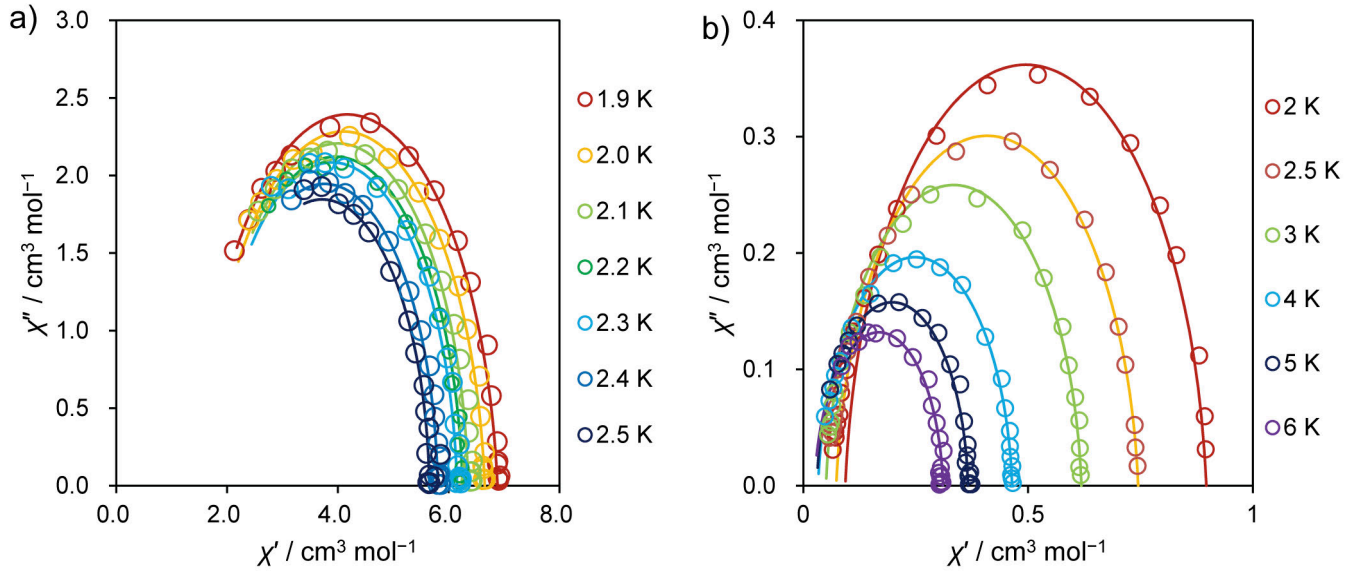

Fig. S7. Cole-Cole plots obtained from the ac susceptibility data under the external dc field of 0.1 T for (a) $\mathbf{I_{Fe}}$ and (b) $\mathbf{I_{Co}}$. Solid lines represent best fits to a generalized Debye model.

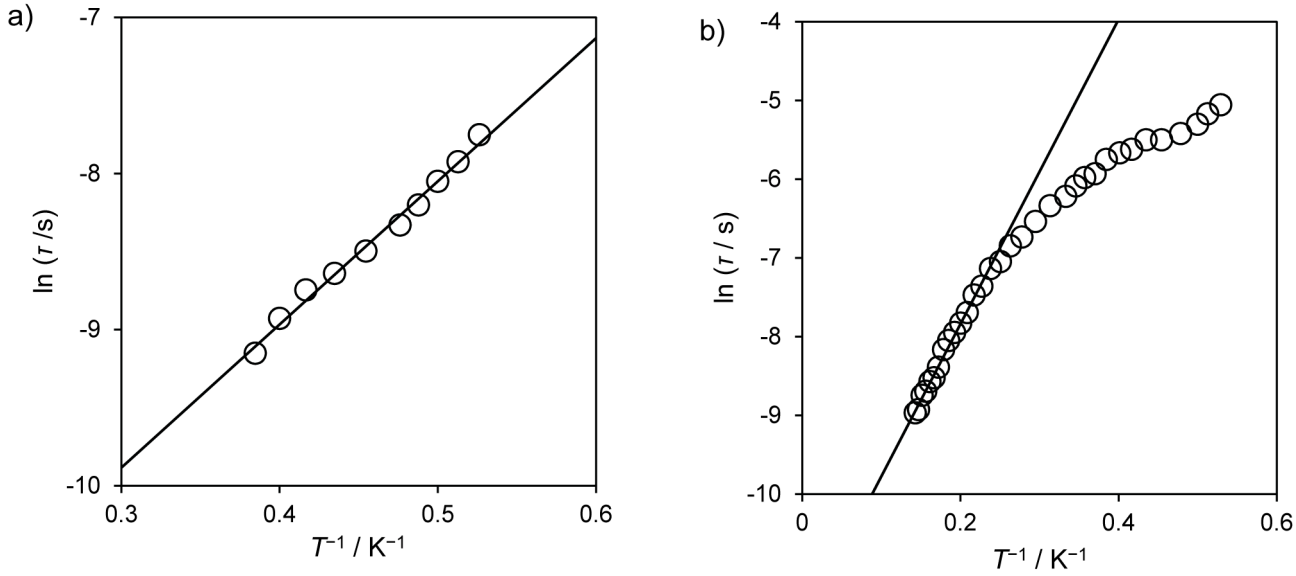

Fig. S8. Plots of relaxation time (τ) versus T^{-1} for (a) $\mathbf{I_{Fe}}$ and (b) $\mathbf{I_{Co}}$ under the external dc field of 0.1 T.

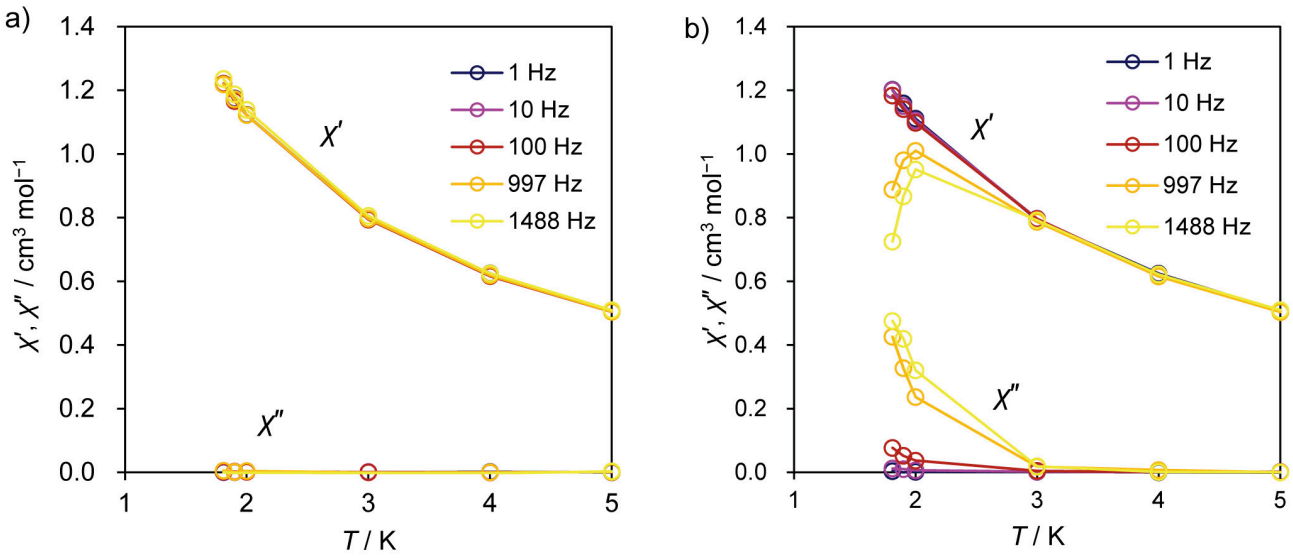

Fig. S9. Temperature dependence of χ' and χ'' for $\mathbf{I_{Mn}}$ under the external dc field of (a) 0 and (b) 0.1 T.

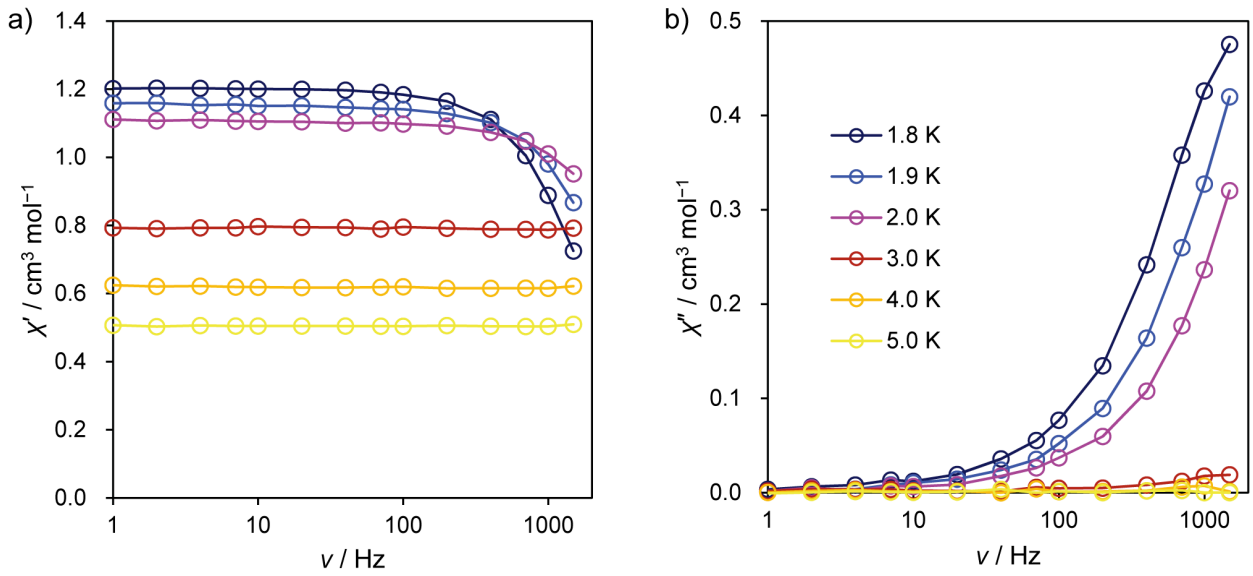

Fig. S10. Frequency dependence of (a) χ' and (b) χ'' for $\mathbf{I_{Mn}}$ under the external dc field of 0.1 T.

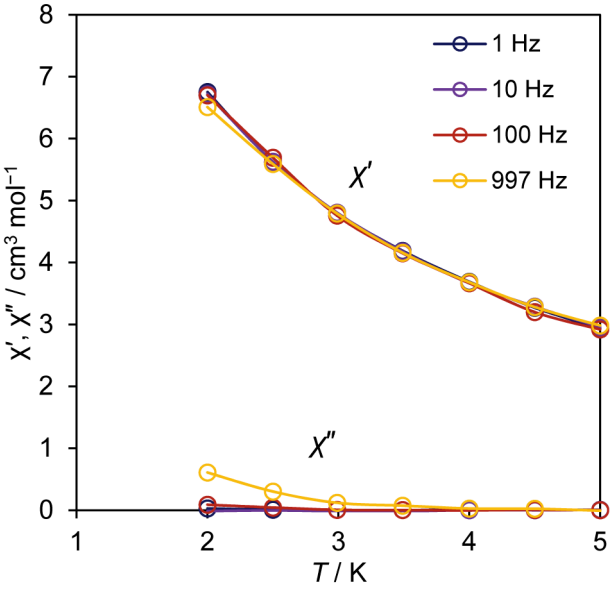

Fig. S11. Temperature dependence of χ' and χ'' for $\mathbf{I_{Fe}}$ under the zero external dc field.

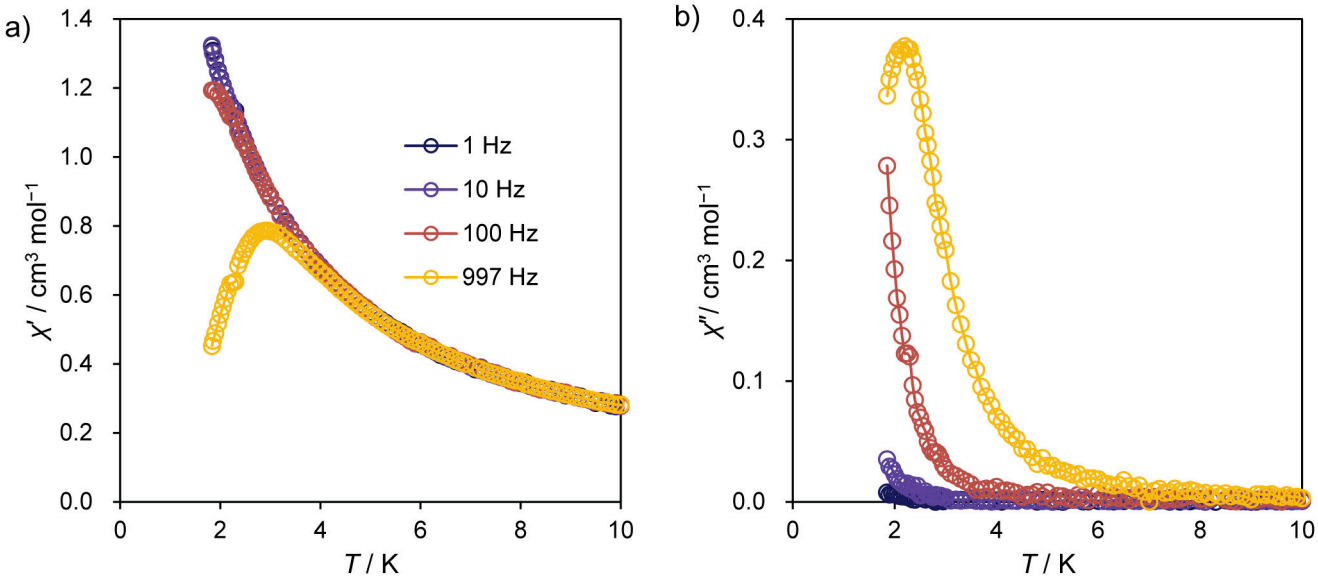

Fig. S12. Temperature dependence of (a) χ' and (b) χ'' for $\mathbf{I_{Fe}}$ under the external dc field of 0.1 T.

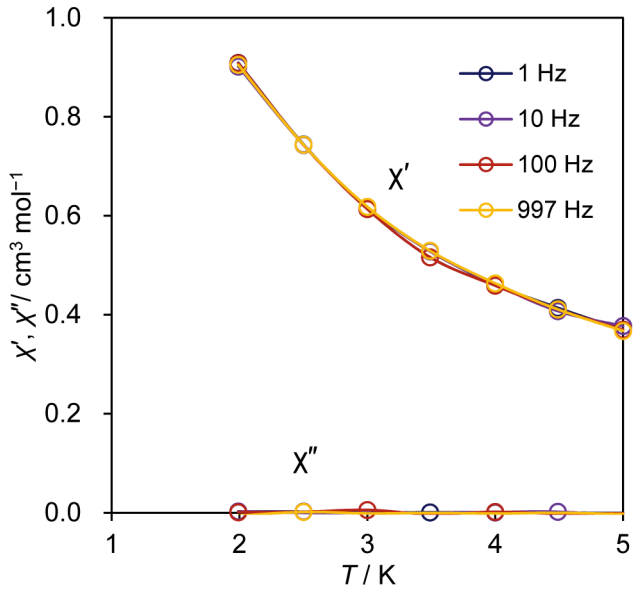

Fig. S13. Temperature dependence of χ' and χ'' for $\mathbf{I_{Co}}$ under the zero external dc field.

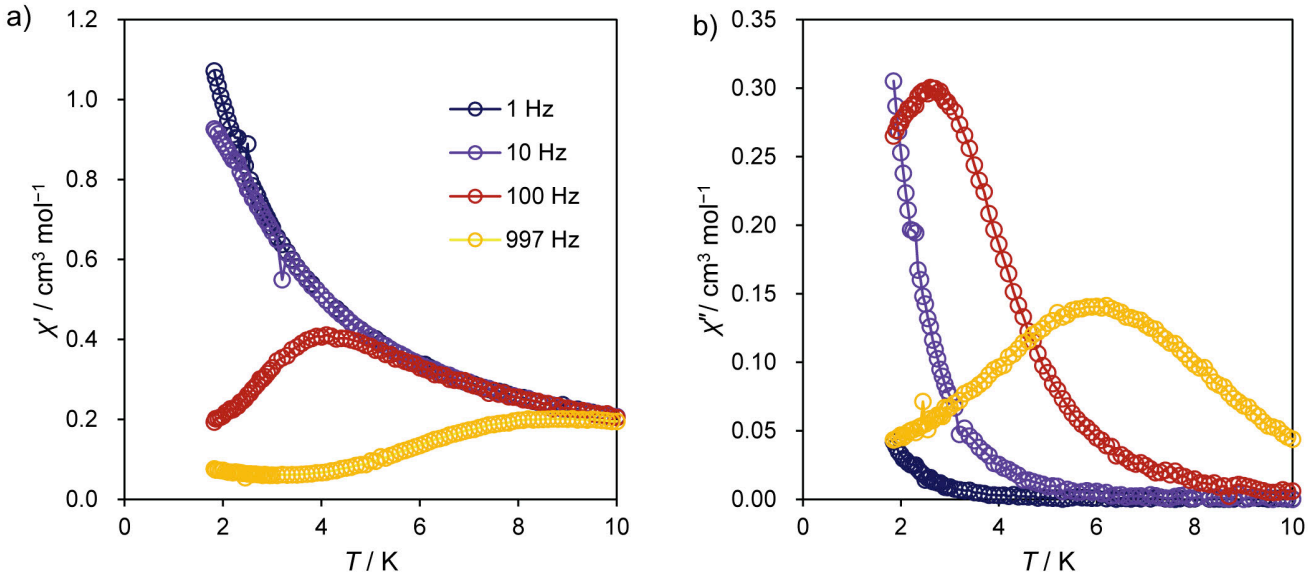

Fig. S14. Temperature dependence of (a) χ' and (b) χ'' for $\mathbf{I_{Co}}$ under the external dc field of 0.1 T.

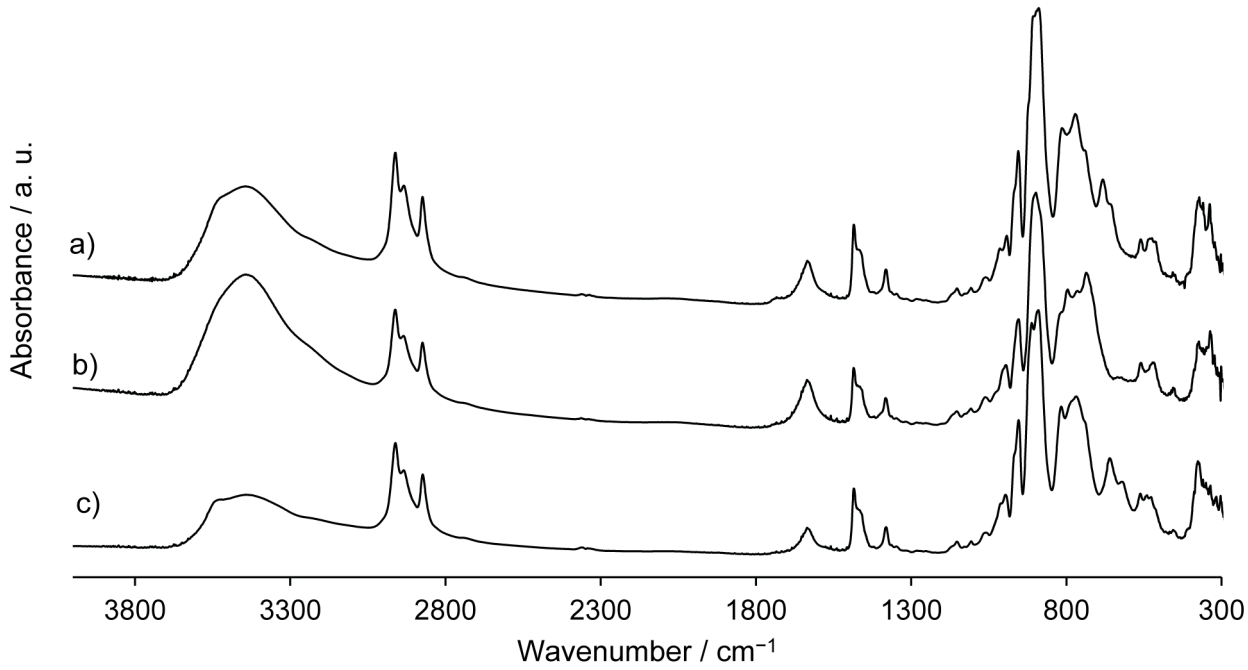

Fig. S15. IR spectra of (a) $\mathbf{I_{Fe}}$, (b) $\mathbf{I_{Co}}$, and (c) $\mathbf{I_{Mn}}$.

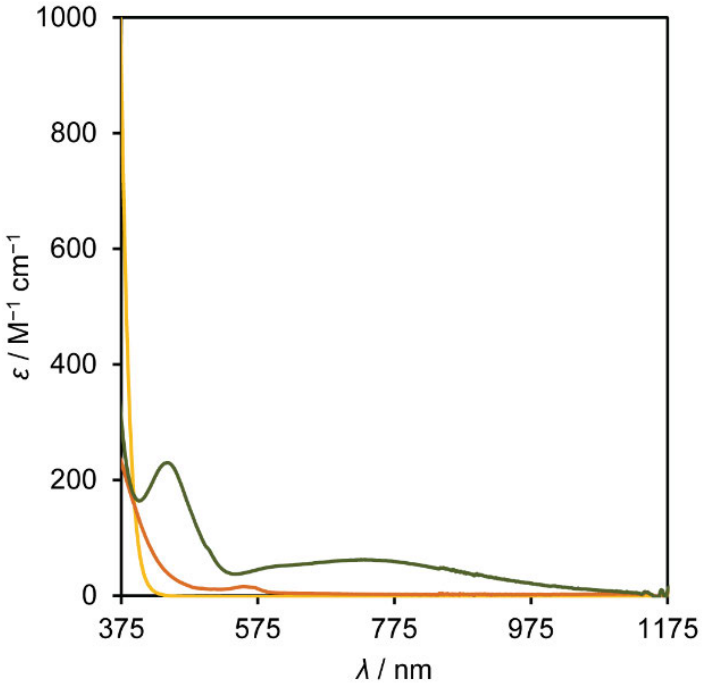

Fig. S16. UV-vis spectra of $\mathbf{I_{Fe}}$ (1.98 mM, yellow line), $\mathbf{I_{Co}}$ (2.01 mM, orange line), and $\mathbf{I_{Mn}}$ (2.06 mM, green line) in acetonitrile (1 cm cell).

Additional References

S1 T. Minato, K. Suzuki, K. Kamata and N. Mizuno, *Chem. –Eur. J.*, 2014, **20**, 5946.

S2 (*a*) *CrystalClear* 1.3.6, Rigaku and Rigaku/MSC, The Woodlands, TX; (*b*) J. W. Pflugrath, *Acta Crystallogr.*, 1999, **D55**, 1718.

S3 Z. Otwinowski and W. Minor, Processing of X-ray Diffraction Data Collected in Oscillation Mode. in *Methods in Enzymology*, C. W. Carter, Jr., R. M. Sweet, Eds., Macromolecular Crystallography, Part A, Academic press, New York, 1997, Vol. 276, pp. 307–326.

S4 *CrystalStructure* 3.8, Rigaku and Rigaku/MSC, The Woodlands, TX.

S5 L. J. Farrugia, *J. Appl. Crystallogr.*, 1999, **32**, 837.

S6 G. M. Sheldrick, SHELX97, *Programs for Crystal Structure Analysis*, Release 97-2, University of Göttingen, Göttingen, Germany, 1997.

S7 Yadokari-XG, Software for Crystal Structure Analyses, K. Wakita 2001; Release of Software (Yadokari-XG 2009) for Crystal Structure Analyses, C. Kabuto, S. Akine, T. Nemoto, E. Kwon, *J. Cryst. Soc. Jpn.* 2009, **51**, 218.

S8 (*a*) I. D. Brown and D. Altermatt, *Acta Crystallogr.*, 1985, **B41**, 244; (*b*) N. E. Brese and M. O'Keeffe, *Acta Crystallogr.*, 1991, **B47**, 192.

S9 Masayuki Koikawa, Hyperfine 2.52, *Program for ESR simulator*, 2006.